ACS OMEGA

Open Access

http://pubs.acs.org/journal/acsodf

Article

Glucose Oxidase Activity Colorimetric Assay Using Redox-Sensitive Electrochromic Nanoparticle-Functionalized Paper Sensors

Taeha Lee, Jeongmin Park, Seung Hyeon Oh, Da Yeon Cheong, Seokbeom Roh, Jae Hyun You, Yoochan Hong,* and Gyudo Lee*

Cite This: *ACS Omega* 2024, 9, 15493−15501

Read Online

ACCESS | Metrics & More | Article Recommendations | Supporting Information

ABSTRACT: Glucose oxidase (GOx) activity assays are vital for various applications, including glucose metabolism estimation and fungal testing. However, conventional methods involve time-consuming and complex procedures. In this study, we present a colorimetric platform for in situ GOx activity measurement utilizing redox-sensitive electrochromic nanoparticles based on polyaniline (PAni). The glucose-adsorbed colorimetric paper sensor, herein termed Glu@CPS, is created by immobilizing ferrocene and glucose onto paper substrates that have been functionalized with PAni nanoparticles. Glu@CPS not only demonstrated rapid detection (within 5 min) but also exhibited remarkable selectivity for GOx and a limit of detection as low as 1.25 μM. Moreover, Glu@CPS demonstrated consistent accuracy in the measurement of GOx activity, exhibiting no deviations even after being stored at ambient temperature for a duration of one month. To further corroborate the effectiveness of this method, we applied Glu@CPS in the detection of GOx activity in a moldy red wine. The results highlight the promising potential of Glu@CPS as a convenient and precise platform for GOx activity measurement in diverse applications including food quality control, environmental monitoring, and early detection of fungal contamination.

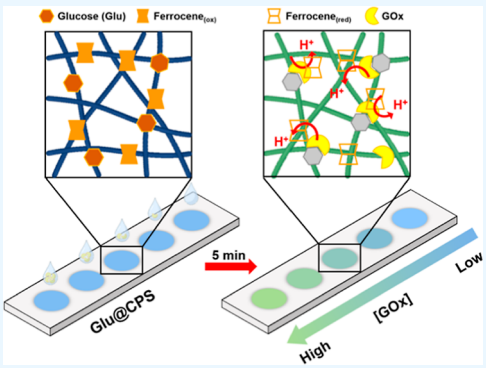

INTRODUCTION

Glucose (Glu) is a vital component of human physiological fluids, with elevated concentrations posing a significant threat to health through the potential onset of diabetes.[1] Consequently, a variety of biosensors for glucose measurement have been developed.[2−5] Among these, glucose oxidase (GOx), produced by fungi such as *Aspergillus niger*, has emerged as a primary enzyme in biosensors for glucose detection.[6−8] GOx not only catalyzes the oxidation of glucose into hydrogen peroxide and d-glucono-δ-lactone but also possesses unique characteristics such as specific activity, thermal stability, pH tolerance, and substrate specificity.[9−14] These attributes have led to widespread utilization and growing interest in GOx across various industrial sectors, including food, clinical diagnostics, and biotechnology. Concurrently, research utilizing GOx is actively progressing. Particularly in the food processing, cosmetics, and pharmaceutical industries, monitoring GOx activity for rapid detection of fungal contamination has become a research focus.[15−20] This approach is crucial not only for ensuring food safety and quality but also for maintaining product integrity within these industries.[21,22]

Traditional methods for GOx activity detection, such as spectrophotometry, chromatography-based techniques, and electrochemical analysis, yield valuable insights but require specialized equipment, extensive expertise, and considerable processing time.[23−27] Additionally, these assays lack the convenience and accessibility required for in situ detection, making them unsuitable for rapid, real-time monitoring of GOx activity. Rapid detection of GOx activity is becoming increasingly important in diverse fields such as medical care, environmental monitoring, food safety, and industrial process control.[28−32] Real-time detection of biological substances, including GOx, is also vital for situations that demand immediate responsiveness.[33,34] A representative example of on-site detection is the colorimetric paper sensor (CPS), characterized by its lightweight, low cost, and ease of use.[35−37] It affords the advantage of simplicity, obviating the need for complicated equipment or expertise.[36,38] The CPS allows for intuitive interpretation of results through color changes, thereby enabling rapid analysis.

The key factors for the development of a CPS suitable for on-site detection are ease of use, short response time, and cost-effectiveness.[39] To fulfill these criteria, it is essential to fabricate a CPS by using appropriate materials. Polyaniline (PAni) is a material that has recently gained attention as one of the

Received: January 10, 2024
Revised: February 23, 2024
Accepted: March 7, 2024
Published: March 20, 2024

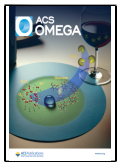

https://doi.org/10.1021/acsomega.4c00335
ACS Omega 2024, 9, 15493−15501

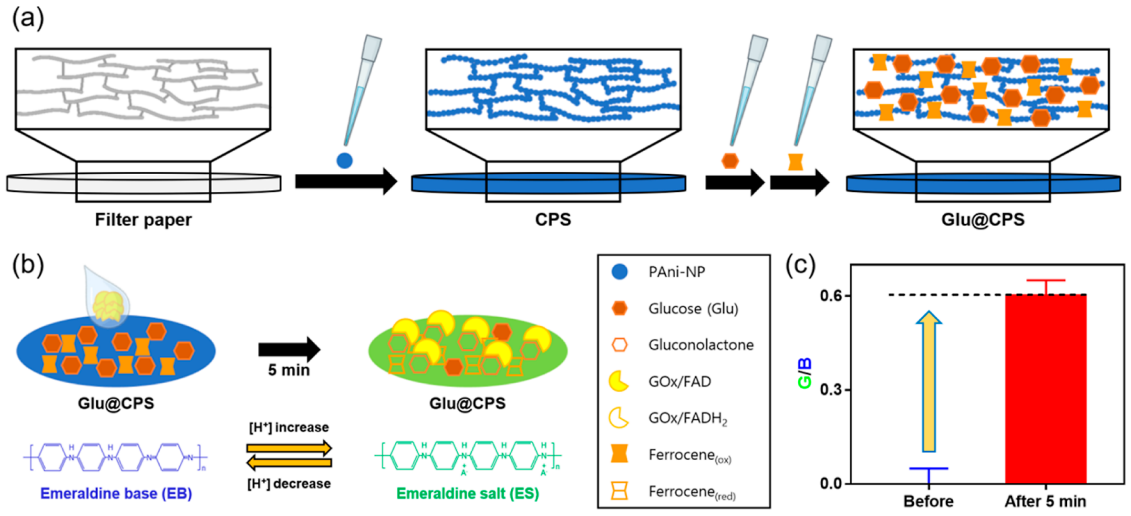

Figure 1. Schematic diagrams of the (a) fabrication procedure of Glu@CPS, (b) color change of Glu@CPS and molecular structure change of PAni according to the enzymatic reaction, and (c) comparison of before and after G/B data of Glu@CPS in the absence and presence of GOx.

electroactive polymers due to its unique properties, including electrical, optical, and environmental stability.[40,41] PAni has numerous applications, especially in sensor technology.[42−47] One primary reason is its redox properties, which lead to color changes during electrochemical reactions.[48] Specifically, PAni nanoparticles (NPs) exhibit distinct color changes when exposed to various pH levels. Under acidic conditions, they appear green, indicating their emeraldine salt form. As the pH shifts toward neutral and basic, they transition to blue, reflecting their emeraldine base form. This electrochromic characteristic makes PAni highly effective in detecting the presence and concentration of specific chemicals or biological substances in colorimetric sensors. Thus, PAni emerges as an ideal material for the rapid on-site detection of crucial substances, such as GOx. Furthermore, ferrocene is another ideal material for the rapid detection of GOx.[49] It comprises two cyclopentadienyl rings bound to a central iron atom in a "sandwich" configuration. Ferrocene has been extensively studied and utilized in the fields of chemistry and electrochemistry because of its redox properties, which remain relatively unaffected by external factors such as pH and temperature.[50] These stable redox properties make ferrocene suitable for various applications, including batteries, fuel cells, sensors, and catalysts.[51−54]

In this study, we developed a glucose-adsorbed CPS (Glu@CPS) functionalized with pH-dependent electrochromic PAni NPs and a redox mediator (i.e., ferrocene) for effective GOx detection. This colorimetric sensor enables rapid analysis of the range of GOx activity in less than 5 min and exhibits a limit of detection (LOD) of 1.25 μM GOx. This innovative approach overcomes the constraints of existing methods, offering a simple and rapid in situ detection system that is apt for scenarios that require immediate GOx activity assessment, such as fungal detection. As a proof-of-concept study, we demonstrated its feasibility in real-world applications by testing the presence of GOx in spoiled red wine. As a result, our assessment is that Glu@CPS presents significant potential as an important tool in a variety of fields in which rapid detection is paramount.

MATERIALS AND METHODS

Materials. Aniline, pectin (Pec), hydrochloric acid (HCl), ammonium persulfate (APS), Whatman 41 filter paper, D-(+)-glucose (Glu), GOx from *A. niger*, ferrocene, phosphate-buffered saline (PBS), ethyl alcohol, fructose (Fru), maltose (Mal), lactose (Lac), sucrose (Suc), lipase, pepsin, pectolyase from *Aspergillus japonicus*, lactate oxidase (LOx), and α-glucosidase were purchased from Sigma-Aldrich (Burlington, MA, USA). Red wine (Alpace, Chile) was purchased from a local grocery store in South Korea.

Synthesis of Polyaniline Nanoparticles. First, a 60 mL aniline-Pec solution was prepared using 1.8 g of Pec, 9 mL of HCl (11 N), and 0.9 g of aniline in pure water. Next, the aniline-Pec solution was incubated at 60 °C for 10 min to dissolve Pec. Then, a 25 mL APS solution containing 2.3 g of APS in pure water was added dropwise to the aniline-Pec solution, and the mixture was stirred continuously for 4 h to synthesize PAni NPs. The resulting PAni NPs were precipitated via 1:1 ethanol−water (500 mL) filtration and subsequently washed with 1:1 ethanol−water (500 mL). Finally, PAni NPs were redispersed by ultrasonication for 5 min. X-ray diffraction (XRD, D8 advance, Bruker, Germany) patterns of the samples were recorded from 2θ 10 to 60° at the step of 0.1 s/step using monochromatic Cu Kα radiation at a 40 kV excitation voltage and a 40 mA tube current (Figure S1a). FTIR characterization of the PAni NPs was carried out using a Nicolet FTIR spectrometer (Thermo Fisher Scientific Inc., USA) (Figure S1b). The morphology of the PAni NPs sample was analyzed by scanning electron microscopy (JSM-6701F, Jeol, Japan) (Figure S1c). High-resolution SEM images were obtained at a high voltage (10 kV). The Au layer (~5 nm in thickness) was coated onto each paper using a sputter coater (108 auto, Cressington Scientific Instruments Inc., UK).

Fabrication of the Glu-Adsorbed CPS. A CPS was fabricated by adsorbing PAni NPs onto Whatman 41 filter paper. The filter paper was dipped in PAni NPs solution (20 mg/mL) and completely dried for 2 h. The soaking and drying steps were repeated five times. The CPS was cut into circles (6 mm in diameter) and placed in PBS (pH = 7.4) before use. Subsequently, Glu@CPS was fabricated as follows. Specifically, 10 μL of Glu solution (40 mg/mL) was dropped onto the center of the CPS. After completely drying, 10 μL of ferrocene

https://doi.org/10.1021/acsomega.4c00335
ACS Omega 2024, 9, 15493−15501

solution (4.5 mg/mL) was dropped (Figure 1a). Glu@CPS was used after it was completely dry.

GOx Detection Using Glu@CPS. GOx solutions were prepared at various concentrations (0.00, 0.01, 0.05, 0.10, 1.00, 5.00, and 10.00 mg/mL) to evaluate the sensitivity and response range of Glu@CPS to GOx. For each concentration, an adequate amount (10 μL) of GOx solution was dropped onto the center of Glu@CPS, and the color change of Glu@CPS was monitored for 5 min (Figure S2). The color of Glu@CPS changes from blue to green in the presence of GOx in the solution, which is related to the pH-sensitive behavior of the PAni NPs. As detailed in Figure 1b, the PAni NPs undergo a distinct color transition in response to changes in the hydrogen ion concentration. Specifically, at lower pH levels (higher hydrogen ion concentration), the NPs exhibit a green hue, indicating the protonated emeraldine salt form of PAni. Conversely, at higher pH levels (lower hydrogen ion concentration), the color shifts to blue, representing the deprotonated emeraldine base form of PAni. Therefore, the colorimetric change in Glu@CPS is a direct response to the enzymatic reaction involving GOx, which alters the local pH and consequently triggers the observable color change in the PAni NPs. These colorimetric responses were analyzed visually and quantitatively using the colorimetric analysis tool (ImageJ).

Glu@CPS Selectivity Test. To evaluate the selectivity performance of Glu@CPS, the sensor was tested against various well-known enzymes including lipase, pepsin, pectolyase, and LOx. Each enzyme solution was prepared at the same concentration (40 mg/mL), and these solutions were then dropped onto the center of Glu@CPS. Following this, the colorimetric response of Glu@CPS to the enzyme solution was monitored.

Darkroom Setup and Data Analysis. Accurate analysis of paper sensors such as Glu@CPS demands a uniform environment that allows controlled manipulation of parameters such as the light source, angle, and shooting equipment. To this end, a custom-designed darkroom was constructed for the uniform and accurate analysis of the CPS. The darkroom is equipped with an internal light source featuring precise brightness control to ensure consistency in results. Furthermore, for optimal CPS analysis, we compared the degree of color change according to the number of light sources and the floor color (Figure S3). Next, CPS shooting was performed within the darkroom using a smartphone (Samsung Galaxy S22 Ultra). The red−green−blue (RGB) values of the captured images and videos were extracted using ImageJ software, followed by an analysis based on the ratio of green/blue (G/B) within the RGB data. A subsequent increase in the G/B value was found to correlate with both the presence and concentration of GOx (Figure 1c). To further enhance the accuracy of CPS analysis, mean values for G and B were quantified within a precisely defined circular area of 6 mm in diameter (380 pixels; Figure S4).

Application in Real Samples. The purchased wine was refrigerated (4 °C) prior to usage. The wine was diluted with PBS to a concentration of 10%. To induce fungal growth and generate moldy wine, 1 mL of the wine was placed in a microtube and incubated at 23 °C for 2 weeks. The presence of fungi in the wine was confirmed by the appearance of black clusters on the surface of the solution.

RESULTS AND DISCUSSION

Characterization of Glu@CPS. Figure S1a shows the XRD pattern of the PAni NPs. The diffractogram of PAni NPs displayed small humps around $2\theta = 25°$, with a corresponding d spacing of 3.41 Å, indicating the periodicity perpendicular to the polymer chain of PAni NPs.[55] Next, we observed the FTIR spectra of PAni NPs. In Figure S1b, the characteristic peaks at 1585 and 1495 cm^{-1} were related to the quinonoid and benzenoid structures, respectively.[56] The bands at 1290 cm^{-1} were assigned to the C−N stretching of the secondary aromatic amine, consistent with the previously known FTIR spectrum of PAni NPs.[57] Furthermore, the morphology of the PAni NPs was analyzed using SEM (Figure S1c).[44]

Principle of Glu@CPS. The scheme for detecting GOx in solution using Glu@CPS is illustrated in Figure 1b. In this protocol, GOx in solution is detected by Glu@CPS. When GOx is present in the solution, it encounters Glu adsorbed on Glu@CPS and undergoes a reduction to produce gluconolactone and hydrogen peroxide (eq 1, Figure S5). This hydrogen peroxide then spontaneously dissociates to generate hydrogen ions (eq 2). After this reaction, reduced GOx can react with another molecule, ferrocene, which is also adsorbed on Glu@CPS (Figure S6). During this process, the reduced GOx interacts with ferrocene and is oxidized, leading to the generation of hydrogen ions (eq 3).[58,59]

$$\text{Glucose} + \text{GOx/FAD} \rightarrow \text{gluconolactone} + \text{GOx/FADH}_2 + \text{H}_2\text{O}_2 \quad (1)$$

$$\text{H}_2\text{O}_2 \rightarrow 2\text{e}^- + \text{O}_2 + 2\text{H}^+ \quad (2)$$

$$\text{GOx/FADH}_2 + 2\text{ferrocene}_{(\text{ox})} \rightarrow \text{GOx/FAD} + 2\text{ferrocene}_{(\text{red})} + 2\text{H}^+ \quad (3)$$

This reaction induces a structural change in the chemistry of PAni NPs adsorbed onto Glu@CPS, resulting in a color transition from blue to green. This transformation can be analyzed either visually or with colorimetric analysis tools. In the absence of GOx or when GOx is inactivated (i.e., denatured), the reduced form of GOx is not generated, thus preventing any electrochromic reaction (Figure S7). We have monitored the detection of GOx using Glu@CPS. As depicted in Figure 1c, upon the addition of a drop of GOx solution, there is an increase in the G/B value shift, signifying the presence of GOx.

Optimization of Glu@CPS Performance Conditions. Previous studies have reported various biosensors for detecting Glu using redox reactions with GOx.[5,44] However, in contrast, measuring GOx using Glu and other sugars has been rarely reported.[60,61] Herein, we tested which saccharides could efficiently recognize GOx. First, Glu@CPS, Fru@CPS, Mal@CPS, Lac@CPS, and Suc@CPS were prepared by coating the CPS with various saccharides, such as Glu, Fru, Mal, Lac, and Suc (Figure S8). The concentration of each saccharide solution was 40 mg/mL. Next, to check whether the saccharide-coated CPS could detect GOx, 10 μL of GOx (10 mg/mL) was dropped onto the center of each CPS. As a result, only the G/B value of Glu@CPS showed a significant increase (i.e., from blue to green), while the other G/B values did not change (i.e., from blue to blue). Specifically, the G/B shift values of Glu@CPS, Fru@CPS, Mal@CPS, Lac@CPS, and Suc@CPS were 0.47 ± 0.04, 0.00 ± 0.01, 0.00 ± 0.00, -0.01 ± 0.01, and 0.00

https://doi.org/10.1021/acsomega.4c00335
ACS Omega 2024, 9, 15493−15501

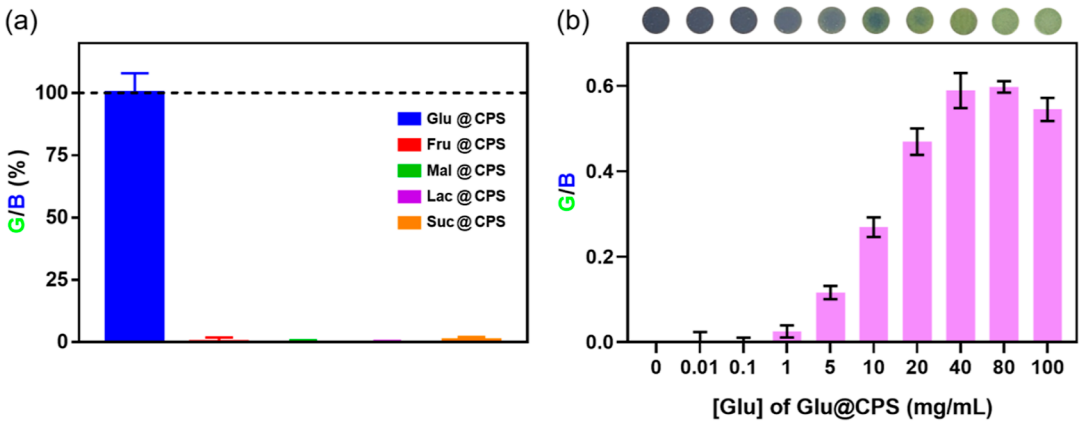

Figure 2. Optimization of Glu on Glu@CPS. (a) Selectivity test of GOx with response to various saccharides. (b) Photographs and the G/B shift for GOx detection through Glu@CPS with different concentrations of Glu solutions.

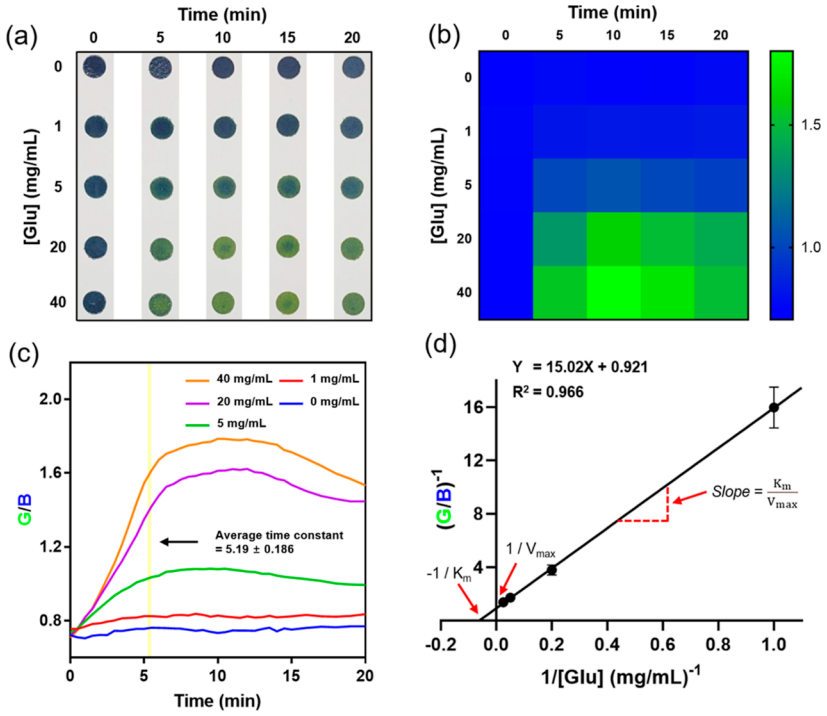

Figure 3. (a) CPS photos and (b) heatmap according to the Glu concentration and reaction time. (c) GOx kinetics analysis using Glu@CPS. The kinetics data were analyzed via video every 30 s, with a GOx concentration of 10 mg/mL. The average time constant was calculated by averaging the time constants of the curves for each Glu concentration (0−4016.31 mg/mL; see Figure S10). (d) Double reciprocal plot of the G/B value and Glu concentration from (c) and Figure S11 (K_m = 0.9 μM ± 1.62 and V_{max} = 1.2 μM min^{-1} ± 0.1).

± 0.01, respectively. To ensure consistent analysis across various saccharide-coated CPSs, the G/B shift values were normalized by using the largest shift observed in Glu@CPS as the reference point, which was set at 100%. Consequently, the other saccharide-coated CPS resulted in the following normalized values: 0.23 ± 1.66% for Fru, −0.14 ± 0.88% for Mal, −0.96 ± 1.43% for Lac, and 0.87 ± 1.29% for Suc (Figure 2a), affirming Glu's suitability for GOx detection.

Also, we optimized the fabrication process of Glu@CPS. In our previous study, we found that when fabricating a CPS, the order of adsorbed materials affects the sensor's performance.[44] Therefore, an additional process was carried out under three conditions (only Glu without ferrocene, ferrocene after Glu, and Glu after ferrocene) on the CPS. Following the addition of the GOx solution onto the three different conditions, the G/B values of each Glu@CPS after 5 min were 0.92 ± 0.01, 1.21 ± 0.01, and 0.97 ± 0.02, respectively (Figure S9). Interestingly, the Glu@CPS that adsorbed ferrocene after Glu adsorption exhibited the most favorable performance. The specific ordering between Glu and ferrocene appears to regulate the redox reaction, resulting in a more pronounced color change. A leading hypothesis is that Glu facilitates ferrocene in the process of electrostatic binding to the CPS. In other words, the additional adsorption of ferrocene occurs smoothly in Glu@CPS.

Next, Glu concentration optimization was conducted to fabricate optimal Glu@CPS. Various Glu concentrations (0−100 mg/mL) were coated on the CPS, and GOx solution (10 μL, 10 mg/mL) was dropped to obtain a G/B shift. As shown in Figure 2b, the G/B shift of Glu@CPS increased with

https://doi.org/10.1021/acsomega.4c00335
ACS Omega 2024, 9, 15493−15501

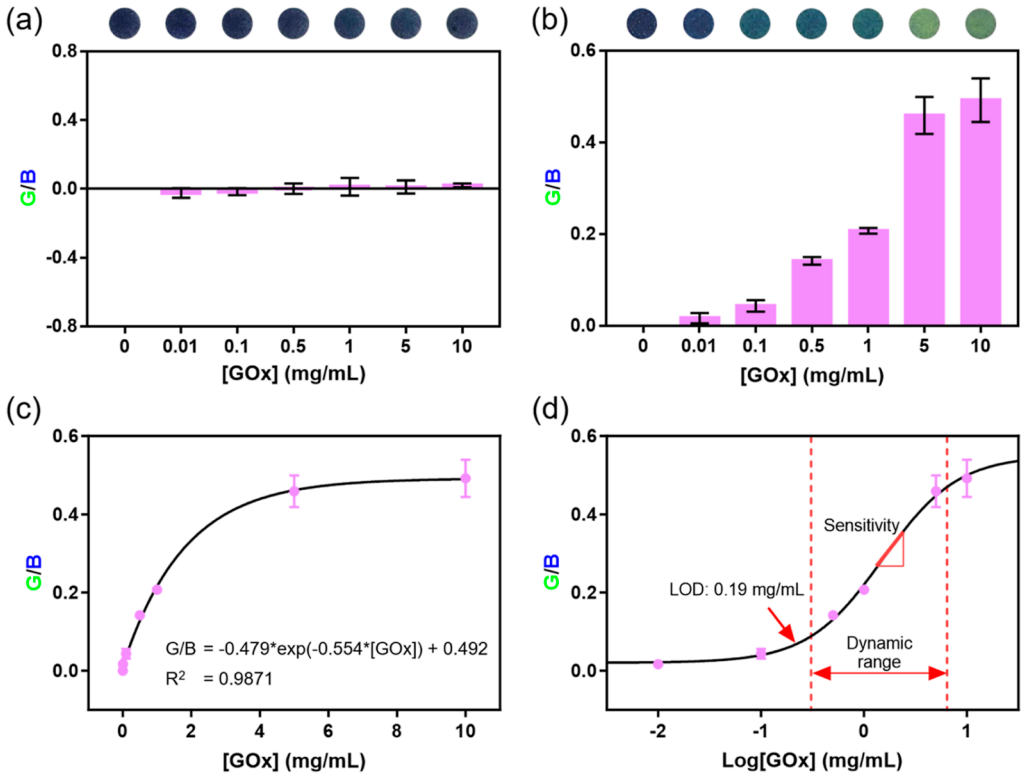

Figure 4. Quantitative Detection of GOx. (a) Photographs and the G/B shift of the CPS without Glu according to the GOx concentration. (b) Photographs and the GOx assay using Glu@CPS. (c) Exponential curve of G/B against the GOx level. (d) Semilog plot showing the sigmoid relationship between the G/B values and GOx concentration from (c), including sensitivity, LOD, and dynamic range. LOD was calculated by $y_{LOD} = \bar{y}_{blank} + 3\sigma_{blank}$. Each data point represents measurements taken in triplicate.

increasing Glu concentration. More specifically, at a given reaction time (5 min), the G/B value increased in correlation with the Glu concentration ranging from 1 to 40 mg/mL and reached saturation at higher concentrations (>40 mg/mL). Hence, the optimal Glu@CPS was produced using a Glu concentration of 40 mg/mL.

To assess the feasibility of Glu@CPS-based GOx kinetics analysis, we designed a 5-by-5 matrix analysis encompassing five distinct Glu concentrations (0, 1, 5, 20, and 40 mg/mL) spanning five different reaction durations (0, 5, 10, 15, and 20 min), as depicted in Figure 3a. We confirmed that the color of the CPS changed more prominently as the adsorbed Glu concentration increased, in line with the findings in Figure 2b. However, intriguingly, the alteration in the CPS color did not directly correlate with the increment in the color change over time. For a comprehensive examination, the G/B values of the CPS in Figure 3a were subjected to heatmap plot analysis (Figure 3b). As a result, the degree of color change did not intensify with longer time intervals; instead, the most significant color change occurred at 10 min, followed by a subsequent decline. This phenomenon can be attributed to the interplay between the redox reaction and water evaporation on the CPS surface. More specifically, as the CPS gradually dries and the solution's concentration undergoes changes, both molecular diffusion and redox reactivity consequently diminish.

To thoroughly examine the phenomenon, we analyzed the kinetics by monitoring every 30 s for a duration of 20 min (Figure 3c). For each Glu concentration, a kinetics curve was acquired, showing a tendency quite similar to the heatmap plot (Figure 3b). The initial slope and final steady-state values in Figure 3c increase depending on the Glu concentration. The optimal GOx detection time was calculated by the saturation point (time constant, τ) in the kinetic curves (Figure S10a).[62] The saturation time point for each concentration (1, 5, 20, and 40 mg/mL) was 3.00, 3.84, 7.60, and 6.33 min, respectively. Based on this result, the Glu@CPS-based GOx analysis time was set to an average time constant of 5 min (Figure S10b).

For further enzymatic kinetics analysis, we considered the Michaelis–Menten model (Figure S10).[63,64] The initial reaction rate (V_o) is usually characterized as the mass of product formed per unit time during the initial phase of the conversion of the substrate to the product. For Glu@CPS, the amount of the product is proportional to the G/B value. V_o was obtained by a linear fit of the initial phase of the curve depicted in Figure 3c. A nonlinear least-squares fit of V_o to the concentration of the substrate (Glu) yields a value of 1.2 μM min^{-1} for the maximum reaction rate (V_{max}), 0.9 μM for the Michaelis–Menten constant (K_m), and 114.7 s^{-1} for the turnover number (k_{cat}). According to the literature, the V_{max}, K_m, and k_{cat} values for the GOx–Glu reaction are reported as 37.8 μM min^{-1}, 4.87 mM, and 9.71 s^{-1}, respectively.[65] This discrepancy arises from the presence of ferrocene adsorbed on Glu@CPS, which enhances the enzymatic reaction of GOx. To facilitate an intuitive comprehension of nonlinear kinetic data, the Lineweaver–Burk plot was utilized,[66] and similar parameter values were obtained (Figures 3d and S10).

Quantitative Detection of GOx Using Glu@CPS. A GOx assay was performed to evaluate the ability of Glu@CPS to detect GOx. Before the GOx assay, we needed to know about the color characteristics of GOx. The color of GOx is either white or yellow, and yellow powder extracted from *A. niger* is generally used. Thus, depending on the concentration,

https://doi.org/10.1021/acsomega.4c00335
ACS Omega 2024, 9, 15493−15501

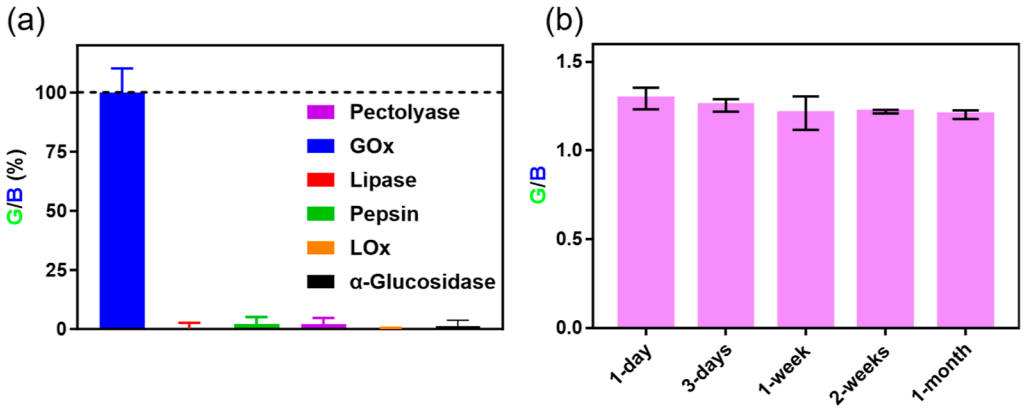

Figure 5. (a) Selectivity assessment of Glu@CPS involving GOx and other enzymes, such as lipase, pepsin, pectolyase, LOx, and α-glucosidase, and (b) long-term stability evaluation of Glu@CPS.

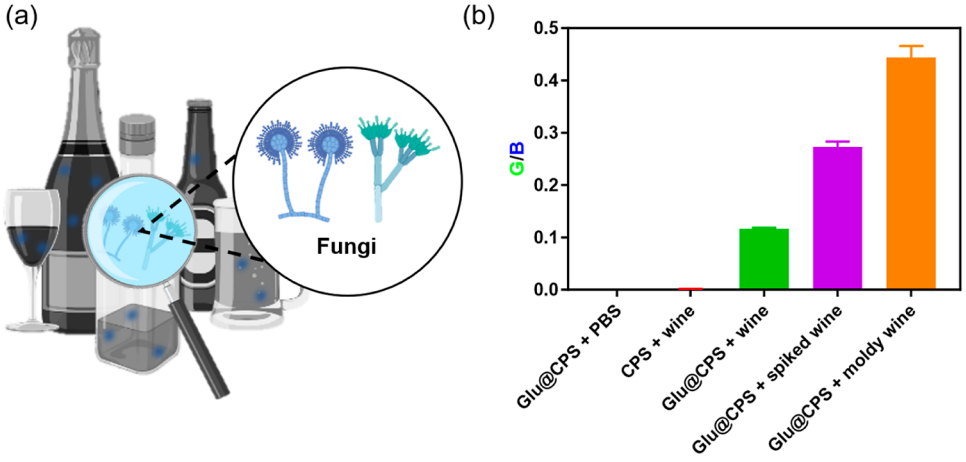

Figure 6. (a) Schematic illustration of fungi in liquors. (b) G/B shift of the reaction with wine samples using Glu@CPS and the CPS.

the color of the GOx solution changes from light yellow to yellow (Figure S12). As our Glu@CPS biosensor relies on color, we explored if variations in the GOx solution color could affect the CPS background color and potentially lead to inaccurate outcomes. Excluding the color change from the Glu-GOx enzymatic reaction, we use the CPS to observe the color change according to the GOx concentration. Figure 4a displays the G/B shift amounts for different GOx concentrations (ranging from 0 to 10 mg/mL). The CPS color without Glu remained consistent across GOx concentrations, with minimal G/B shifts, indicating no impact from the GOx color. Moreover, we assessed Glu@CPS's capability toward GOx (ranging from 0 to 10 mg/mL). The G/B value of Glu@CPS rapidly increased, as depicted in Figure 4b,c, exhibiting a strong correlation (R^2 = 0.987) with the concentration of GOx. Using a semilogarithmic plot (Figure 4d), we determined the performance metrics of Glu@CPS in terms of sensitivity, LOD, and dynamic range,[67] yielding results of 0.4 $(mg/mL)^{-1}$, 0.19 mg/mL (1.25 μM), and a GOx range of 0.3−6.5 mg/mL, respectively. The performance of Glu@CPS is comparable with that of other GOx detection methods and is summarized in Table S1.

Selectivity and Stability of Glu@CPS. We performed a selectivity and stability performance analysis of Glu@CPS. The selectivity of Glu@CPS to GOx was investigated by testing with various enzymes (lipase, pepsin, pectolyase, and LOx). The proposed enzymes, commonly used in the food industry, were selected based on their potential copresence in the food to be detected. As shown in Figure 5a, a distinct color change (i.e., blue to green) was only observed in GOx, whereas other enzymes exerted no influence on the Glu@CPS color change (G/B shift). The G/B shifts of Glu@CPS reacted with lipase, pepsin, pectolyase, LOx, and α-glucosidase were 0.00 ± 0.02, 0.01 ± 0.01, 0.01 ± 0.01, −0.02 ± 0.02, and −0.02 ± 0.00, respectively. This showed insignificant color changes of −0.45 ± 3.51%, 2.12 ± 2.92%, 1.95 ± 2.73%, −3.23 ± 3.67%, and 1.21 ± 2.52% compared to those of the G/B shift when reacted with GOx. These results demonstrated that the proposed Glu@CPS shows excellent selectivity for GOx detection. Subsequently, to evaluate the stability of Glu@CPS, the sensor was stored in a dry state at 23 °C for different durations (1, 3, 7, 14, and 30 days). For each Glu@CPS, 10 μL of GOx solution (10 mg/mL) was dropped onto the center, and the color change of Glu@CPS was monitored at 5 min (Figure 5b). The G/B values of Glu@CPS reacted for varying durations were 1.29 ± 0.05, 1.25 ± 0.03, 1.21 ± 0.08, 1.22 ± 0.01, and 1.20 ± 0.02, respectively. Surprisingly, the performance of Glu@CPS stored for a month showed minimal change in comparison to Glu@CPS stored for only 1 day. This can be attributed to the absence of easily denatured biological elements (such as proteins) in the produced Glu@CPS. In addition, the stability of the sensor was measured over long-term storage (14 days) at various temperatures (4, 23, and 60 °C), relative humidities (20, 30, and 50%), and pH conditions

https://doi.org/10.1021/acsomega.4c00335
ACS Omega 2024, 9, 15493−15501

(pH 3, 7, and 9) (Figure S13). As a result, the performance of Glu@CPS under each condition was 96.8, 96.6, 95.5, 94.0, 97.3, and 96.1%, respectively. This means that the stability of Glu@CPS is excellent, even after long periods of time. In essence, Glu@CPS can be stored at room temperature for a prolonged duration, making it well-suited for on-site detection.

Quantification of GOx in Real Samples. To investigate the practical utility of Glu@CPS, we attempted to detect GOx in alcoholic beverages, where fungi are prone to form (Figure 6a). Wine samples were purchased from a local market and diluted in 10% PBS. These samples were tested under various conditions to evaluate the performance of Glu@CPS in wine (Figure 6b). First, since wine has its own color (red), we tested whether the color of wine affects the CPS. Upon reacting wine with the CPS, the G/B shift was 0.00 ± 0.02, indicating a minimal color change. Next, we checked the reaction of Glu@CPS with three types of wine (pure, spiked, and moldy). The spiked wine was supplemented with GOx at a concentration of 1 mg/mL, while the moldy wine was allowed to develop mold by being stored at 23 °C for 2 weeks. For the pure wine, a slight G/B shift (0.11 ± 0.00) was observed, likely due to the minimal amount of GOx present. G/B shifts were 0.27 ± 0.01 and 0.44 ± 0.02 for spiked and moldy wines, respectively. Surprisingly, for the spiked wines, the G/B shift was similar to the result (G/B shift at 1 mg/mL GOx concentration) observed in Figure 4b. Interesting results were also observed in moldy wine with a G/B shift of approximately 0.44 ± 0.02. The G/B shift of moldy wine can be calculated at about 5 mg/mL of GOx. This indicates that GOx was secreted by the fungi in the wine. This suggests that the proposed Glu@CPS is capable of detecting GOx produced by fungi in actual samples.

CONCLUSIONS

In summary, we fabricated Glu@CPS, capable of selective and rapid detection of GOx within 5 min. This was achieved by adsorbing redox-sensitive NPs (i.e., PAni NPs), redox mediators (ferrocene), and glucose (Glu) onto filter paper. Glu@CPS can detect GOx concentrations as low as 1.25 μM and exhibits a strong correlation at 0.3−6.5 mg/mL GOx. Additionally, Glu@CPS demonstrated stability for one month of storage at room temperature. It was also effective in detecting the presence of GOx in moldy wine, thereby illustrating its practical utility in real-world applications. Certainly, additional research is required to conduct a broader analysis of various beverages and foods. The Glu@CPS can serve as a valuable on-site monitoring tool for GOx activity, facilitating swift quantification of GOx in the food, cosmetics, and pharmaceutical industries. We believe that by applying a variety of adsorbed metabolites, not just glucose, this approach will offer a new paradigm for the detection of pathogens (e.g., bacteria and fungi) through the identification of various enzymes.

ASSOCIATED CONTENT

Supporting Information

The Supporting Information is available free of charge at https://pubs.acs.org/doi/10.1021/acsomega.4c00335.

Characterization of PAni NPs; dripping solution volume range; darkroom optimization; G/B value measurement range changes; glucose oxidation chemical equation; ferrocene chemical structure; GOx activity test; saccharides chemical structures; Glu@CPS fabrication order performance difference; exponential G/B shift model with saturation points; Michaelis−Menten kinetics model fitting of Glu@CPS data; GOx solution color variation by concentration; Glu@CPS stability test; and comparison of various methods with our work for the detection of GOx (PDF)

AUTHOR INFORMATION

Corresponding Authors

Yoochan Hong − *Department of Medical Device, Korea Institute of Machinery and Materials (KIMM), Daegu 42994, South Korea;* orcid.org/0000-0002-6345-9877; Email: ychong1983@kimm.re.kr

Gyudo Lee − *Department of Biotechnology and Bioinformatics, Korea University, Sejong 30019, South Korea; Interdisciplinary Graduate Program for Artificial Intelligence Smart Convergence Technology, Korea University, Sejong 30019, South Korea;* orcid.org/0000-0001-7895-5112; Email: lkd0807@korea.ac.kr

Authors

Taeha Lee − *Department of Biotechnology and Bioinformatics, Korea University, Sejong 30019, South Korea; Interdisciplinary Graduate Program for Artificial Intelligence Smart Convergence Technology, Korea University, Sejong 30019, South Korea*

Jeongmin Park − *Department of Biotechnology and Bioinformatics, Korea University, Sejong 30019, South Korea*

Seung Hyeon Oh − *Department of Biotechnology and Bioinformatics, Korea University, Sejong 30019, South Korea; Interdisciplinary Graduate Program for Artificial Intelligence Smart Convergence Technology, Korea University, Sejong 30019, South Korea*

Da Yeon Cheong − *Department of Biotechnology and Bioinformatics, Korea University, Sejong 30019, South Korea; Interdisciplinary Graduate Program for Artificial Intelligence Smart Convergence Technology, Korea University, Sejong 30019, South Korea*

Seokbeom Roh − *Department of Biotechnology and Bioinformatics, Korea University, Sejong 30019, South Korea; Interdisciplinary Graduate Program for Artificial Intelligence Smart Convergence Technology, Korea University, Sejong 30019, South Korea*

Jae Hyun You − *Division of Convergence Business, Korea University, Sejong 30019, South Korea*

Complete contact information is available at: https://pubs.acs.org/10.1021/acsomega.4c00335

Author Contributions

T.L. and J.P. contributed equally to this work. The manuscript was written through contributions of all authors. All authors have given approval to the final version of the manuscript.

Notes

The authors declare no competing financial interest.

ACKNOWLEDGMENTS

This work was supported by the National Research Foundation of Korea (2021R1C1C1012822) and the Korea Institute of Machinery & Materials (KIMM) (NK250E). This work was also supported by the Ministry of Health and Welfare (HG23C1598000023). This work was also supported by the Ministry of Science and ICT (00258971). This study was also

supported by a Korea University grant, Korea University Insung Research Grant, and the BK21 FOUR (Fostering Outstanding Universities for Research). Following are results of a study on the "Leaders in INdustry-university Cooperation 3.0" Project, supported by the Ministry of Education and National Research Foundation of Korea.

REFERENCES

(1) Wang, J. Electrochemical Glucose Biosensors. *Chem. Rev.* **2008**, *108* (2), 814−825.
(2) Qiao, Y.; Liu, Q.; Lu, S.; Chen, G.; Gao, S.; Lu, W.; Sun, X. High-performance non-enzymatic glucose detection: using a conductive Ni-MOF as an electrocatalyst. *J. Mater. Chem. B* **2020**, *8* (25), 5411−5415.
(3) Xie, F.; Cao, X.; Qu, F.; Asiri, A. M.; Sun, X. Cobalt nitride nanowire array as an efficient electrochemical sensor for glucose and H2O2 detection. *Sens. Actuators, B* **2018**, *255*, 1254−1261.
(4) Wei, M.; Qiao, Y.; Zhao, H.; Liang, J.; Li, T.; Luo, Y.; Lu, S.; Shi, X.; Lu, W.; Sun, X. Electrochemical non-enzymatic glucose sensors: recent progress and perspectives. *Chem. Commun.* **2020**, *56* (93), 14553−14569.
(5) Jang, J. W.; Kim, H.; Kim, I.; Lee, S. W.; Jung, H. G.; Hwang, K. S.; Lee, J. H.; Lee, G.; Lee, D.; Yoon, D. S. Surface Functionalization of Enzyme-Coronated Gold Nanoparticles with an Erythrocyte Membrane for Highly Selective Glucose Assays. *Anal. Chem.* **2022**, *94* (17), 6473−6481.
(6) Mandpe, P.; Prabhakar, B.; Gupta, H.; Shende, P. Glucose oxidase-based biosensor for glucose detection from biological fluids. *Sens. Rev.* **2020**, *40* (4), 497−511.
(7) Chen, T.; Liu, D.; Lu, W.; Wang, K.; Du, G.; Asiri, A. M.; Sun, X. Three-Dimensional Ni2P Nanoarray: An Efficient Catalyst Electrode for Sensitive and Selective Nonenzymatic Glucose Sensing with High Specificity. *Anal. Chem.* **2016**, *88* (16), 7885−7889.
(8) Hao, S.; Zhang, H.; Sun, X.; Zhai, J.; Dong, S. A mediator-free self-powered glucose biosensor based on a hybrid glucose/MnO2 enzymatic biofuel cell. *Nano Res.* **2021**, *14* (3), 707−714.
(9) Wong, C. M.; Wong, K. H.; Chen, X. D. Glucose oxidase: natural occurrence, function, properties and industrial applications. *Appl. Microbiol. Biotechnol.* **2008**, *78* (6), 927−938.
(10) Bankar, S. B.; Bule, M. V.; Singhal, R. S.; Ananthanarayan, L. Glucose oxidase—An overview. *Biotechnol. Adv.* **2009**, *27* (4), 489−501.
(11) Golikova, E. P.; Lakina, N. V.; Grebennikova, O. V.; Matveeva, V. G.; Sulman, E. M. A study of biocatalysts based on glucose oxidase. *Faraday Discuss.* **2017**, *202* (0), 303−314.
(12) Fan, E.; Shi, P.; Zhang, X.; Lin, J.; Wu, F.; Li, L.; Chen, R. Glucose oxidase-based biocatalytic acid-leaching process for recovering valuable metals from spent lithium-ion batteries. *Waste Manage.* **2020**, *114*, 166−173.
(13) Adams, E. C.; Mast, R. L.; Free, A. H. Specificity of glucose oxidase. *Arch. Biochem. Biophys.* **1960**, *91* (2), 230−234.
(14) Bauer, J. A.; Zámocká, M.; Majtán, J.; Bauerová-Hlinková, V. Glucose Oxidase, an Enzyme "Ferrari": Its Structure, Function, Production and Properties in the Light of Various Industrial and Biotechnological Applications. *Biomolecules* **2022**, *12* (3), 472.
(15) Khatami, S. H.; Vakili, O.; Ahmadi, N.; Soltani Fard, E.; Mousavi, P.; Khalvati, B.; Maleksabet, A.; Savardashtaki, A.; Taheri-Anganeh, M.; Movahedpour, A. Glucose oxidase: Applications, sources, and recombinant production. *Biotechnol. Appl. Biochem.* **2022**, *69* (3), 939−950.
(16) Fu, L.-H.; Qi, C.; Lin, J.; Huang, P. Catalytic chemistry of glucose oxidase in cancer diagnosis and treatment. *Chem. Soc. Rev.* **2018**, *47* (17), 6454−6472.
(17) Fang, M.; Grant, P. S.; McShane, M. J.; Sukhorukov, G. B.; Golub, V. O.; Lvov, Y. M. Magnetic Bio/Nanoreactor with Multilayer Shells of Glucose Oxidase and Inorganic Nanoparticles. *Langmuir* **2002**, *18* (16), 6338−6344.
(18) Kim, I.; Kwon, D.; Lee, D.; Lee, T. H.; Lee, J. H.; Lee, G.; Yoon, D. S. A highly permselective electrochemical glucose sensor using red blood cell membrane. *Biosens. Bioelectron.* **2018**, *102*, 617−623.
(19) Kim, I.; Kwon, D.; Lee, D.; Lee, G.; Yoon, D. S. Permselective glucose sensing with GLUT1-rich cancer cell membranes. *Biosens. Bioelectron.* **2019**, *135*, 82−87.
(20) Kim, I.; Kim, C.; Lee, D.; Lee, S. W.; Lee, G.; Yoon, D. S. A bio-inspired highly selective enzymatic glucose sensor using a red blood cell membrane. *Analyst* **2020**, *145* (6), 2125−2132.
(21) Dubey, M. K.; Zehra, A.; Aamir, M.; Meena, M.; Ahirwal, L.; Singh, S.; Shukla, S.; Upadhyay, R. S.; Bueno-Mari, R.; Bajpai, V. K. Improvement Strategies, Cost Effective Production, and Potential Applications of Fungal Glucose Oxidase (GOD): Current Updates. *Front. Microbiol.* **2017**, *8*, 1032.
(22) Galant, A. L.; Kaufman, R. C.; Wilson, J. D. Glucose: Detection and analysis. *Food Chem.* **2015**, *188*, 149−160.
(23) Samukaite-Bubniene, U.; Mazetyte-Stasinskiene, R.; Chernyakova, K.; Karpicz, R.; Ramanavicius, A. Time-resolved fluorescence spectroscopy based evaluation of stability of glucose oxidase. *Int. J. Biol. Macromol.* **2020**, *163*, 676−682.
(24) Naderi Asrami, P.; Mozaffari, S. A.; Saber Tehrani, M.; Aberoomand Azar, P. A novel impedimetric glucose biosensor based on immobilized glucose oxidase on a CuO-Chitosan nanobiocomposite modified FTO electrode. *Int. J. Biol. Macromol.* **2018**, *118*, 649−660.
(25) Singh, R.; Musameh, M.; Gao, Y.; Ozcelik, B.; Mulet, X.; Doherty, C. M. Stable MOF@enzyme composites for electrochemical biosensing devices. *J. Mater. Chem. C* **2021**, *9* (24), 7677−7688.
(26) Kucherenko, I. S.; Soldatkin, O. O.; Dzyadevych, S. V.; Soldatkin, A. P. Electrochemical biosensors based on multienzyme systems: Main groups, advantages and limitations—A review. *Anal. Chim. Acta* **2020**, *1111*, 114−131.
(27) Ning, D.; Liu, Q.; Wang, Q.; Du, X.-M.; Ruan, W.-J.; Li, Y. Luminescent MOF nanosheets for enzyme assisted detection of H2O2 and glucose and activity assay of glucose oxidase. *Sens. Actuators, B* **2019**, *282*, 443−448.
(28) Haleem, A.; Javaid, M.; Singh, R. P.; Suman, R.; Rab, S. Biosensors applications in medical field: A brief review. *Sensor. Int.* **2021**, *2*, 100100.
(29) Zhang, J.; Huang, H.; Song, G.; Huang, K.; Luo, Y.; Liu, Q.; He, X.; Cheng, N. Intelligent biosensing strategies for rapid detection in food safety: A review. *Biosens. Bioelectron.* **2022**, *202*, 114003.
(30) Ahmed, S. R.; Chand, R.; Kumar, S.; Mittal, N.; Srinivasan, S.; Rajabzadeh, A. R. Recent biosensing advances in the rapid detection of illicit drugs. *Trac. Trends Anal. Chem.* **2020**, *131*, 116006.
(31) Dincer, C.; Bruch, R.; Costa-Rama, E.; Fernández-Abedul, M. T.; Merkoçi, A.; Manz, A.; Urban, G. A.; Güder, F. Disposable Sensors in Diagnostics, Food, and Environmental Monitoring. *Adv. Mater.* **2019**, *31* (30), 1806739.
(32) Qin, X.; Liu, J.; Zhang, Z.; Li, J.; Yuan, L.; Zhang, Z.; Chen, L. Microfluidic paper-based chips in rapid detection: Current status, challenges, and perspectives. *Trac. Trends Anal. Chem.* **2021**, *143*, 116371.
(33) Choi, J. R. Development of Point-of-Care Biosensors for COVID-19. *Front. Chem.* **2020**, *8*, 517.
(34) Campuzano, S.; Pedrero, M.; Gamella, M.; Serafín, V.; Yáñez-Sedeño, P.; Pingarrón, J. M. Beyond Sensitive and Selective Electrochemical Biosensors: Towards Continuous, Real-Time, Anti-biofouling and Calibration-Free Devices. *Sensors* **2020**, *20* (12), 3376.
(35) Umapathi, R.; Sonwal, S.; Lee, M. J.; Mohana Rani, G.; Lee, E.-S.; Jeon, T.-J.; Kang, S.-M.; Oh, M.-H.; Huh, Y. S. Colorimetric based on-site sensing strategies for the rapid detection of pesticides in agricultural foods: New horizons, perspectives, and challenges. *Coord. Chem. Rev.* **2021**, *446*, 214061.
(36) Erdemir, S.; Malkondu, S. On-site and low-cost detection of cyanide by simple colorimetric and fluorogenic sensors: Smartphone and test strip applications. *Talanta* **2020**, *207*, 120278.

https://doi.org/10.1021/acsomega.4c00335
ACS Omega 2024, 9, 15493−15501

(37) Xu, J.; Chen, X.; Khan, H.; Yang, L. A dual-readout paper-based sensor for on-site detection of penicillinase with a smartphone. *Sens. Actuators, B* **2021**, *335*, 129707.
(38) Li, A.; Li, H.; Ma, Y.; Wang, T.; Liu, X.; Wang, C.; Liu, F.; Sun, P.; Yan, X.; Lu, G. Bioinspired laccase-mimicking catalyst for on-site monitoring of thiram in paper-based colorimetric platform. *Biosens. Bioelectron.* **2022**, *207*, 114199.
(39) Umapathi, R.; Park, B.; Sonwal, S.; Rani, G. M.; Cho, Y.; Huh, Y. S. Advances in optical-sensing strategies for the on-site detection of pesticides in agricultural foods. *Trends Food Sci. Technol.* **2022**, *119*, 69−89.
(40) Boeva, Z. A.; Sergeyev, V. G. Polyaniline: Synthesis, properties, and application. *Polym. Sci., Ser. C* **2014**, *56* (1), 144−153.
(41) Geniès, E.; Boyle, A.; Lapkowski, M.; Tsintavis, C. Polyaniline: A historical survey. *Synth. Met.* **1990**, *36* (2), 139−182.
(42) Kim, H. J.; Park, I.; Pack, S. P.; Lee, G.; Hong, Y. Colorimetric Sensing of Lactate in Human Sweat Using Polyaniline Nanoparticles-Based Sensor Platform and Colorimeter. *Biosensors* **2022**, *12* (4), 248.
(43) Hong, Y.; Kim, H. S.; Lee, T.; Lee, G.; Kwon, O. Polyaniline Nanoskein: Synthetic Method, Characterization, and Redox Sensing. *Nanoscale Res. Lett.* **2020**, *15* (1), 215.
(44) Lee, T.; Kim, I.; Cheong, D. Y.; Roh, S.; Jung, H. G.; Lee, S. W.; Kim, H. S.; Yoon, D. S.; Hong, Y.; Lee, G. Selective colorimetric urine glucose detection by paper sensor functionalized with polyaniline nanoparticles and cell membrane. *Anal. Chim. Acta* **2021**, *1158*, 338387.
(45) Lee, T.; Lee, H.-T.; Hong, J.; Roh, S.; Cheong, D. Y.; Lee, K.; Choi, Y.; Hong, Y.; Hwang, H.-J.; Lee, G. A regression-based machine learning approach for pH and glucose detection with redox-sensitive colorimetric paper sensors. *Anal. Methods* **2022**, *14* (46), 4749−4755.
(46) Kim, Y.; Lee, T.; Kim, M.; Park, S.; Hu, J.; Lee, K.; Hong, Y.; Park, I.; Lee, G. Fast Responsive, Reversible Colorimetric Nanoparticle-Hydrogel Complexes for pH Monitoring. *Nanomaterials* **2022**, *12* (22), 4081.
(47) Lee, T.; Kim, C.; Kim, J.; Seong, J. B.; Lee, Y.; Roh, S.; Cheong, D. Y.; Lee, W.; Park, J.; Hong, Y.; Lee, G. Colorimetric Nanoparticle-Embedded Hydrogels for a Biosensing Platform. *Nanomaterials* **2022**, *12* (7), 1150.
(48) Thakur, B.; Amarnath, C. A.; Mangoli, S. H.; Sawant, S. N. Polyaniline nanoparticle based colorimetric sensor for monitoring bacterial growth. *Sens. Actuators, B* **2015**, *207*, 262−268.
(49) van Staveren, D. R.; Metzler-Nolte, N. Bioorganometallic Chemistry of Ferrocene. *Chem. Rev.* **2004**, *104* (12), 5931−5986.
(50) Astruc, D. Why is Ferrocene so Exceptional? *Eur. J. Inorg. Chem.* **2017**, *2017* (1), 6−29.
(51) Neuse, E. W. Macromolecular Ferrocene Compounds as Cancer Drug Models. *J. Inorg. Organomet. Polym. Mater.* **2005**, *15* (1), 3−31.
(52) Carraher, C. E. Condensation Metallocene Polymers. *J. Inorg. Organomet. Polym. Mater.* **2005**, *15* (1), 121−145.
(53) Abd-El-Aziz, A. S.; Agatemor, C.; Etkin, N. Sandwich Complex-Containing Macromolecules: Property Tunability Through Versatile Synthesis. *Macromol. Rapid Commun.* **2014**, *35* (5), 513−559.
(54) Hadadpour, M.; Gwyther, J.; Manners, I.; Ragogna, P. J. Multifunctional Block Copolymer: Where Polymetallic and Polyelectrolyte Blocks Meet. *Chem. Mater.* **2015**, *27* (9), 3430−3440.
(55) Amarnath, C. A.; Venkatesan, N.; Doble, M.; Sawant, S. N. Water dispersible Ag@polyaniline-pectin as supercapacitor electrode for physiological environment. *J. Mater. Chem. B* **2014**, *2* (31), 5012−5019.
(56) Brožová, L.; Holler, P.; Kovářová, J.; Stejskal, J.; Trchová, M. The stability of polyaniline in strongly alkaline or acidic aqueous media. *Polym. Degrad. Stab.* **2008**, *93* (3), 592−600.
(57) Elayappan, V.; Murugadoss, V.; Angaiah, S.; Fei, Z.; Dyson, P. J. Development of a conjugated polyaniline incorporated electrospun poly(vinylidene fluoride-co-hexafluoropropylene) composite membrane electrolyte for high performance dye-sensitized solar cells. *J. Appl. Polym. Sci.* **2015**, *132* (45), 42777.
(58) Suzuki, N.; Lee, J.; Loew, N.; Takahashi-Inose, Y.; Okuda-Shimazaki, J.; Kojima, K.; Mori, K.; Tsugawa, W.; Sode, K. Engineered Glucose Oxidase Capable of Quasi-Direct Electron Transfer after a Quick-and-Easy Modification with a Mediator. *Int. J. Mol. Sci.* **2020**, *21* (3), 1137.
(59) Chaubey, A.; Malhotra, B. D. Mediated biosensors. *Biosens. Bioelectron.* **2002**, *17* (6−7), 441−456.
(60) Palestino, G.; Legros, R.; Agarwal, V.; Pérez, E.; Gergely, C. Functionalization of nanostructured porous silicon microcavities for glucose oxidase detection. *Sens. Actuators, B* **2008**, *135* (1), 27−34.
(61) Qu, F.; Guo, X.; Liu, D.; Chen, G.; You, J. Dual-emission carbon nanodots as a ratiometric nanosensor for the detection of glucose and glucose oxidase. *Sens. Actuators, B* **2016**, *233*, 320−327.
(62) Lazzarini, E.; Pace, A.; Trozzi, I.; Zangheri, M.; Guardigli, M.; Calabria, D.; Mirasoli, M. An Origami Paper-Based Biosensor for Allergen Detection by Chemiluminescence Immunoassay on Magnetic Microbeads. *Biosensors* **2022**, *12* (10), 825.
(63) Maini, P. K.; Schnell, S. A Century of Enzyme Kinetics: Reliability of the K M and v max Estimates. *Comments Theor. Biol.* **2003**, *8*, 169−187.
(64) Tao, Z.; Raffel, R. A.; Souid, A. K.; Goodisman, J. Kinetic studies on enzyme-catalyzed reactions: oxidation of glucose, decomposition of hydrogen peroxide and their combination. *Biophys. J.* **2009**, *96* (7), 2977−2988.
(65) Luo, W.; Zhu, C.; Su, S.; Li, D.; He, Y.; Huang, Q.; Fan, C. Self-Catalyzed, Self-Limiting Growth of Glucose Oxidase-Mimicking Gold Nanoparticles. *ACS Nano* **2010**, *4* (12), 7451−7458.
(66) Orosco, M. M.; Pacholski, C.; Sailor, M. J. Real-time monitoring of enzyme activity in a mesoporous silicon double layer. *Nat. Nanotechnol.* **2009**, *4* (4), 255−258.
(67) De Acha, N.; Elosúa, C.; Arregui, F. J. Development of an Aptamer Based Luminescent Optical Fiber Sensor for the Continuous Monitoring of Hg2+ in Aqueous Media. *Sensors* **2020**, *20* (8), 2372.

https://doi.org/10.1021/acsomega.4c00335
ACS Omega 2024, 9, 15493−15501